Gating versus doping: Quality parameters of two-dimensional electron systems in undoped and doped GaAs/AlGaAs heterostructures

S. Peters,* L. Tiemann, C. Reichl, and W. Wegscheider
Solid State Physics Laboratory, ETH Zurich, 8093 Zurich, Switzerland
(Received 27 January 2016; published 8 July 2016)

We present an experimental study of the scattering mechanisms in a two-dimensional electron system which is either fully induced by the field effect or resulting from remote doping. The quality criteria—the electron mobility, the quantum scattering time, and the number and development of certain fractional quantum Hall states—are analyzed and compared. By eliminating the scattering off remote ionized impurities (RI) in undoped systems, we can identify the density regimes most susceptible to RI scattering and their impact on the formation of fractional quantum Hall states.

DOI: 10.1103/PhysRevB.94.045304

I. INTRODUCTION

Two-dimensional electron systems (2DES) of high quality can exhibit a variety of exotic quantum effects, such as fractional quantum Hall (FQH) states [1–3] that arise at low temperatures and large perpendicular magnetic fields. Scattering at remote ionized impurities (RI) has been ascertained to impede the formation of various fragile FQH states including the topologically protected 5/2 state [4–6]. It has been shown that above a mobility threshold of around $10^6\,\mathrm{cm^2\,V^{-1}\,s^{-1}}$, intentional ionized dopants, constituting RI, are the source of disorder dictating the emergence or absence of these fragile quantum states. Particular quantum-well doping schemes [5–8] or particular low-temperature sample-illumination protocols [9,10] have been used to suppress the detrimental effects of RI scattering through the formation of a screening layer. Band engineering was also employed by Gamez and Muraki [9] who varied the aluminum content to enhance the screening effect of the fraction of dopants that are not ionized and observed a strong impact on the fragile 5/2 state. All these attempts to cancel out the destructive effects of RI scattering can be circumvented in undoped heterojunction insulated gate field-effect transistors (HIGFETs) [11–15], which allow to detect pronounced FQH states, particularly the 5/2 state [16,17]. The nonexistence of RI in HIGFETs has elucidated the role of further scattering sources such as background impurities (BI) and interface roughness [17–19]. Whereas FQH states are highly affected by remote ionized impurities, in current high-quality GaAs/AlGaAs heterostructures, the electron mobility is predominantly limited by BI [6,20,21], which reside at the location of the 2DES.

In this paper, we investigate the impact of RI scattering on the *quality* [22] of a 2DES residing at the single interface of an undoped GaAs/AlGaAs heterostructure. For this purpose, a HIGFET structure is compared to an alike modulation-doped field-effect transistor (MODFET) structure in terms of mobility and its density dependence, revealing the dominant scattering mechanism. Shubnikov-de Haas (SdH) oscillations at low magnetic field are analyzed regarding quantum scattering time and effective mass. We focus on the low-density regime, where RI are screened to a minor degree. Eventually, the effect of absent RI scattering on the number and development of fractional quantum Hall states is presented.

*peters@phys.ethz.ch

II. THEORY AND METHODS

The quantities evaluated in terms of the sample quality are dominated by distinct scattering mechanisms and are therefore differently affected by remote impurities. The electron mobility μ is given by the ratio of the drift velocity v of the electrons in the 2DES to the applied electric field E across the sample. According to the Drude model [23], the mobility is related to the zero-field transport scattering time τ_t by $\mu \equiv v/E = e \cdot \tau_t/m^\star$, with the electronic charge e and the effective mass $m^\star$. In general, the classical transport scattering time τ_t is defined by [24–26]

$$\tau_t^{-1} = \int f(\theta)(1-\cos\theta)\,d\theta\ , \tag{1}$$

giving more weight to large-angle scattering events, which notably reduce the momentum $p = m^\star v$. The probability of scattering with the angle θ is given by $f(\theta)$. The zero-field transport scattering time determines the conductivity and thus the resistivity at zero magnetic field, $\rho_0 = m^\star/ne^2\tau_t$, where n is the electron density. From the mobility-density dependence $\mu(n)$, the scattering process limiting the mobility can be deduced. The mobility shows a power law dependence on the electron density in the form of

$$\mu \propto n^\alpha\ , \tag{2}$$

where the value of the exponent α is related to the dominant scattering mechanism. It takes the value $\alpha = 1.5$ [26,27] if the mobility is limited by RI scattering, $\alpha = 0.5$[1] for dominant BI scattering, and becomes negative ($\alpha < 0$) for limiting interface-roughness scattering [28,29].

[1]With increasing density, values up to $\alpha = 1$ have been detected for mobilities limited by BI scattering (Ref. [20]; Appl. Phys. Lett. **54**, 2100 (1989)), i.e., the screening becomes weaker with increasing density (peculiarity of 2D screening [Rev. Mod. Phys. **54**, 437 (1982); Phys. Rev. B **69**, 195305 (2004)]); $\alpha \approx 0.6$ for $n \leqslant 1 \times 10^{11}\,\mathrm{cm^{-2}}$ (Refs. [45,46]), and $\alpha \approx 0.7$ for $n \approx 1$–$2 \times 10^{11}\,\mathrm{cm^{-2}}$ (Ref. [21]; Phys. Rev. Lett. **94**, 136401 (2005); Phys. Rev. Lett. **90**, 056806 (2003); Appl. Phys. Lett. **55**, 1888 (1989)).

In contrast to τ_t [Eq. (1)], all scattering events equally contribute to the quantum scattering or single-particle relaxation time τ_q [24–26],

$$\tau_q^{-1} = \int f(\theta)\, d\theta \ , \tag{3}$$

including small-angle scattering, which hardly changes the electron momentum. The quantum scattering time is related to the single-particle level broadening Γ_q due to electron-impurity interaction [30,31], according to

$$\Gamma_q = \frac{\hbar}{2\tau_q} \ . \tag{4}$$

Thus the quantum scattering time determines the density of states (DOS) [26] at finite magnetic field. In the presence of scattering, it defines the time frame during which an electronic momentum eigenstate exists [25]. Since the longitudinal magnetoresistivity ρ_{xx} is connected to the DOS, the quantum scattering time can be extracted from the amplitude of the Shubnikov-de Haas (SdH) oscillations of ρ_{xx} at low magnetic field. In the low-field region (no spin splitting), the field dependence of ρ_{xx} is given by [32]

$$\rho_{xx} \propto \frac{1}{\tau_t} D(E_F) \ , \tag{5}$$

where $D(E_F)$ is the DOS at the Fermi level E_F. At low magnetic field, the SdH oscillations can be approximated by Fourier series expansion of the quantized DOS. If the Landau-level broadening Γ_q is independent of energy and can be described by a Lorentzian, the fundamental harmonic component results in an oscillating magnetoresitance, expressed in the (Ando-) Lifshitz-Kosevich (LK) formula [33–35]

$$\rho_{xx} = \rho_0 \left[1 + 2 \exp\left(-\frac{\pi}{\omega_c \tau_q} \right) \frac{\chi}{\sinh(\chi)} \cos\left(2\pi \frac{E_F}{\hbar \omega_c} \right) \right] , \tag{6}$$

with the cyclotron frequency $\omega_c = eB/m^\star$. The amplitude is damped by disorder, represented by the Dingle [36] factor $\exp(-\pi/\omega_c\tau_q)$, and by temperature T according to the term $\chi/\sinh(\chi)$ with $\chi = 2\pi^2 k_B T/\hbar\omega_c$, containing the Boltzmann constant k_B. The prefactor 2 of the second addend in Eq. (6) is associated with the Fourier representation and is based on a transport scattering rate τ_t^{-1} independent of $D(E_F)$, which is equivalent to a linear dependence of ρ_{xx} on $D(E_F)$ [Eq. (5)]. A linear dependence of τ_t^{-1} and thus a quadratic one of ρ_{xx} on $D(E_F)$ yields an additional factor 2 (see Refs. [37–41]). It has been shown that in certain cases the DOS at finite magnetic field (Landau levels) is Gaussian shaped [32,40,41], resulting in a replacement of the exponential term in Eq. (6) by $\exp(-\pi^2/2\omega_c^2\tau_q^2)$.

Given an effective mass and under the premise that both $m^\star$ and τ_q are temperature independent, based on the magnetic-field dependence of ρ_{xx} according to Eq. (6), the quantum scattering time at a fixed temperature can be extracted from the slope of the plot $\ln(\Delta\rho_{xx}/\rho_0 \times \sinh(\chi)/\chi)$ versus B^{-1}; $\Delta\rho_{xx}$ represents the SdH oscillation amplitude. The intercept of this plot should provide information about the mentioned prefactor of the second addend [42]. The effective mass can be deduced from the temperature dependence of ρ_{xx} at fixed magnetic field, by fitting to $\ln(\Delta\rho_{xx}/T)$ as a function of T (cf. Ref. [43]).

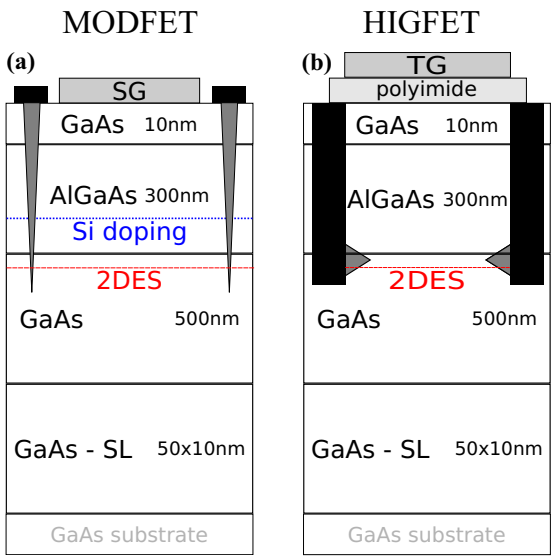

FIG. 1. (a) Doped MODFET structure with surface gate (SG) and Ohmics (black) evaporated on the surface and annealed (vertical diffusion depicted in dark gray). The doping concentration of $1.4 \times 10^{12}\,\mathrm{cm}^{-2}$ at a setback distance of 70 nm has resulted in a 2D electron density of $2.4 \times 10^{10}\,\mathrm{cm}^{-2}$ at 0 V surface-gate voltage. (b) Equivalent undoped HIGFET structure with insulated top gate (TG) and recessed Ohmics, based on lateral diffusion.

The ratio of transport to quantum scattering time gives insight about the dominant scattering mechanism [26,31]. According to the "rule of thumb" of Ref. [19], a ratio of $\tau_t/\tau_q \geqslant 10$ reveals that small-angle scattering at smooth RI potential dominates, and predominant large-angle scattering at sharp BI potential yields $\tau_t/\tau_q \leqslant 10$.

III. STRUCTURES

For this comparative study, we investigated simple single-interface GaAs/AlGaAs heterostructures in Hall-bar geometry. The MODFET structure is provided with a Ti/Au surface gate, and standard AuGe Ohmic contacts are evaporated and annealed [Fig. 1(a)]. In the HIGFET structure, the 2DES is induced by means of a Ti/Au top gate atop an insulating polyimide layer [Fig. 1(b)]. As the electrons forming the 2DES at the GaAs/AlGaAs interface when a bias voltage is applied, originate from the Ohmic contacts, the top gate has to overlap the contact region, which demands recessed Ohmic contacts [14,44] and a lateral diffusion to the interface. To keep all parameters affecting the 2DES quality as constant as possible and thus ensure the best possible comparability, the investigated single-interface heterostructures were consecutively grown in the same molecular beam epitaxy system.

IV. DATA ANALYSIS AND ASSESSMENT

Electron mobility

Figure 2(a) compares the mobility in the MODFET and the HIGFET structure as a function of the electron density.

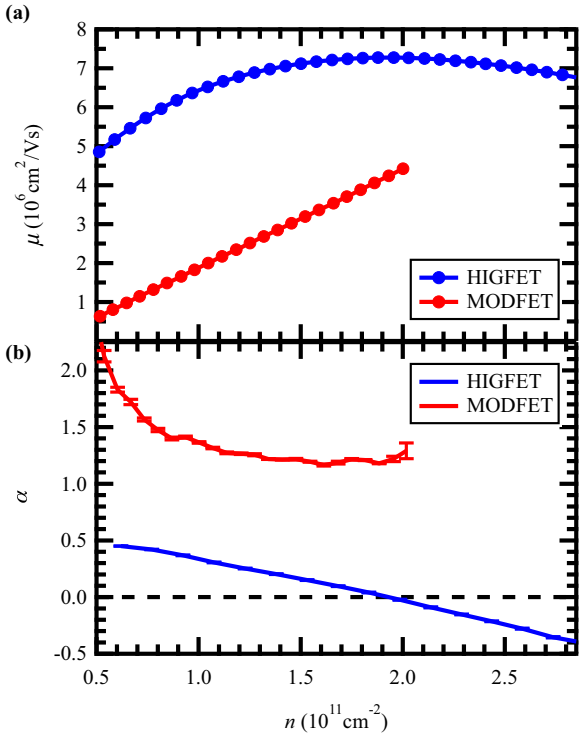

FIG. 2. (a) Mobility-density dependence of the 2DES in the MODFET (red) and HIGFET (blue) structure ($T = 280$ mK). (b) Resulting α parameter as a function of electron density. The α values were gained as the linear slope of the $\log_{10}(\mu)$ vs $\log_{10}(n)$ plot, averaged over overlapping density ranges of 3×10^{10} cm^{-2} width.

In both structures, the minimal accessible density is of the order of 5×10^{10} cm^{-2}. The density increase in the MODFET structure by means of a surface gate is limited by the Schottky barrier; the maximum density is 2×10^{11} cm^{-2}. In contrast, the insulated gate of the HIGFET structure facilitates densities of about 3×10^{11} cm^{-2} before hysteretic effects occur. This hysteresis—not the breakdown of the top gate—constrains the HIGFET's functionality at even higher densities. Within the whole accessible density range, the electrons residing at the single interface of the undoped structure show a significantly higher mobility than those of the modulation-doped structure. The difference substantially increases with decreasing electron density, equivalent to a weaker screening, from a factor 1.6 at high densities to a factor 8.3 at the lowest densities. From the change of mobility with density, the dominant mobility limiting scattering mechanism was deduced according to Eq. (2). The resulting exponent of $\alpha \approx 1.5$ as depicted in Fig. 2(b) reveals that the MODFET structure is dominated by RI over the entire density range. Due to the consecutive growth, the densities of BI are comparable in both structures. In the absence of RI, the contribution of these BI becomes the mobility limiting factor, reflected by $\alpha \approx 0.5$ at low density, consistent with Refs. [45,46]. Increasing the density based on a higher top-gate voltage coincides with a rising penetration of the electron wave function into the AlGaAs barrier. Therefore the roughness of the GaAs/AlGaAs interface becomes more important in terms of mobility limitation and eventually dominant at a density of $n \gtrsim 2 \times 10^{11}$ cm^{-2}, where the α parameter changes sign. A Fourier analysis (cf. Appendix A 2, Fig. 7) excludes the occupation of the second 2D subband as an origin of this decrease in mobility.

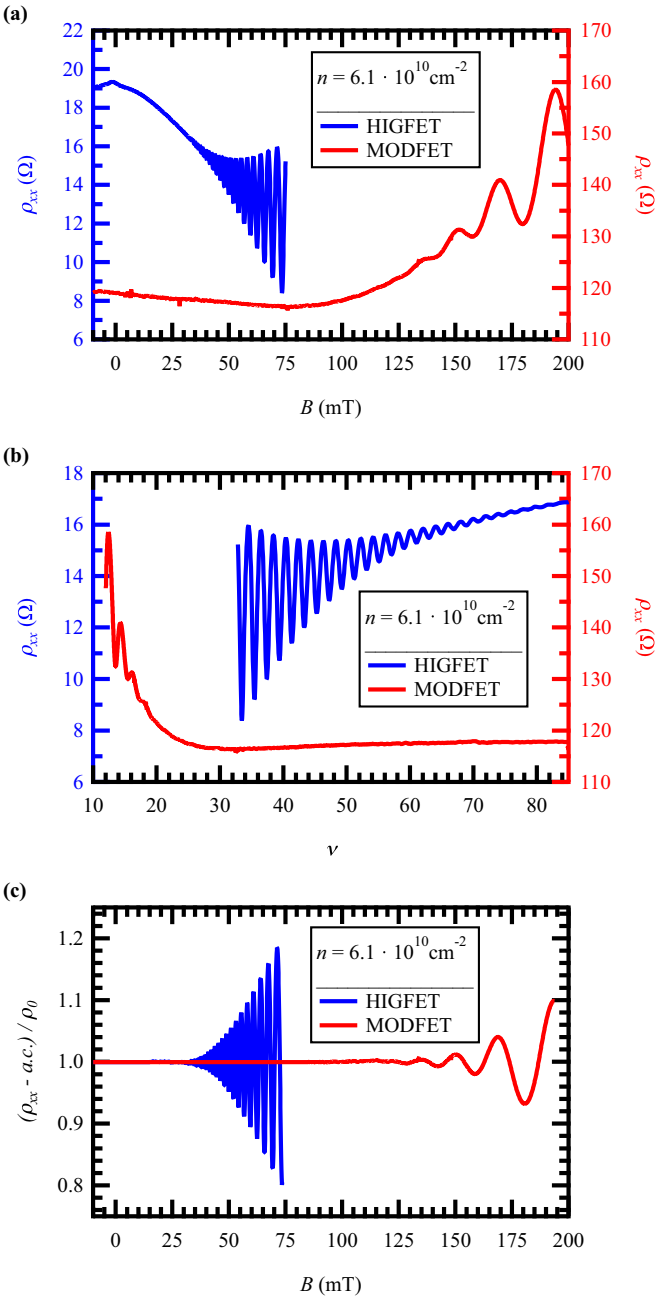

FIG. 3. Comparison of SdH oscillations in the HIGFET (blue) and the MODFET (red) structure; as a function of (a) magnetic field and (b) filling factor, and (c) reduced by additional contributions (a.c.) (cf. main text) as well as normalized to ρ_0.

A. Quantum scattering time

Focusing on the low-field regime, Fig. 3 demonstrates the appearance of SdH oscillations at significantly lower magnetic fields in the HIGFET structure, which is also the case at higher electron densities than the one shown ($n = 6.1 \times 10^{10}$ cm^{-2}). At this density, in the HIGFET structure, the oscillations start

at 30 mT, whereas the corresponding onset in the MODFET structure is at roughly 120 mT [Fig. 3(a)]. Accordingly, distinctly higher filling factors can be resolved—in terms of numbers, up to $\nu \approx 80$ in the HIGFET, as compared to $\nu \leqslant 20$ in the MODFET structure [Fig. 3(b)]. In Fig. 3(c), additional contributions [47–50] to the measured resistivity around zero magnetic field are removed, and the oscillation amplitudes of both structures are normalized. The division by the scaling prefactor ρ_0 at comparable densities eliminates the mobility impact and reveals those of effective mass and quantum scattering time. According to Eq. (6), the larger normalized amplitude of the HIGFET structure at even lower magnetic fields reveals a longer τ_q and/or a reduced $m^\star$. Both quantities will be further examined in the following.

From the amplitude of the SdH oscillations, we deduced the effective mass $m^\star$ and the quantum scattering time τ_q by means of two consecutive fitting procedures. The amplitude $\Delta\rho_{xx}$ [cf. Eq. (6)] can be factorized into one temperature independent and one temperature dependent factor:

$$\Delta\rho_{xx} = F(B)\,\frac{\chi}{\sinh(\chi)}\,. \tag{7}$$

The magnetic-field dependent and temperature independent factor $F(B)$ is given by

$$F_L(B) = 2c\rho_0 \exp(-\pi/\omega_c\tau_q) \tag{8}$$

for a Lorentzian shaped DOS and by

$$F_G(B) = 2c\rho_0 \exp\left(-\pi^2/2\omega_c^2\tau_q^2\right) \tag{9}$$

in the case of a Gaussian shape of the DOS. The additional correction factor c included in Eqs. (8) and (9) considers a deviation of the measured resistivity at zero field from the actual value of ρ_0 as well as a possible factor 2 in case $\rho_{xx} \propto D(E_F)^2$. The actually measured resistivity at zero field may differ from the prefactor ρ_0 in Eq. (6), which does not consider additional contributions [47–50] around $B = 0$, but there is a constant factor between both quantities for constant electron concentration [50].

Analyzing the temperature dependence of the SdH minima at magnetic fields between 75 and 100 mT, the examined temperature range of 300 mK $\leqslant T \leqslant$ 700 mK ensures $\chi \geqslant 2$ for all SdH minima [cf. Fig. 4(b)]; therefore the term $\chi/\sinh(\chi)$ in Eq. (7) can be approximated by $2\chi\exp(-\chi)$. The corresponding linear fit to $\ln(\Delta\rho_{xx}/T)$ versus T [cf. Fig. 4(a)] delivers an effective mass of the electrons in the HIGFET structure of $m^\star = (0.0575 \pm 0.001)\,m_e$. This reduction of $m^\star$ by 14% at a density of $n = 6.1 \times 10^{10}\,\mathrm{cm}^{-2}$ in a HIGFET structure matches the observations in Refs. [51,52] and is of a slightly higher extent. The density-dependent analysis in Ref. [51], supported by the calculations in Ref. [53], yields a mass reduction just at intermediate densities but an enhancement at very low densities. The effective mass reduction is strong evidence for electron-electron interaction [54–57], which can result in an exchange enhancement of the Landau level separation [58]. Figure 4(b) confirms the mass reduction by showing that the temperature dependence of the oscillation minima collapses into $\chi/\sinh(\chi)$ with $\chi = \chi(m^\star = 0.0575\,m_e)$ whereas it does not for $m^\star = 0.067\,m_e$. In contrast, the electrons in the MODFET structure do not have a reduced effective mass, and the temperature dependence

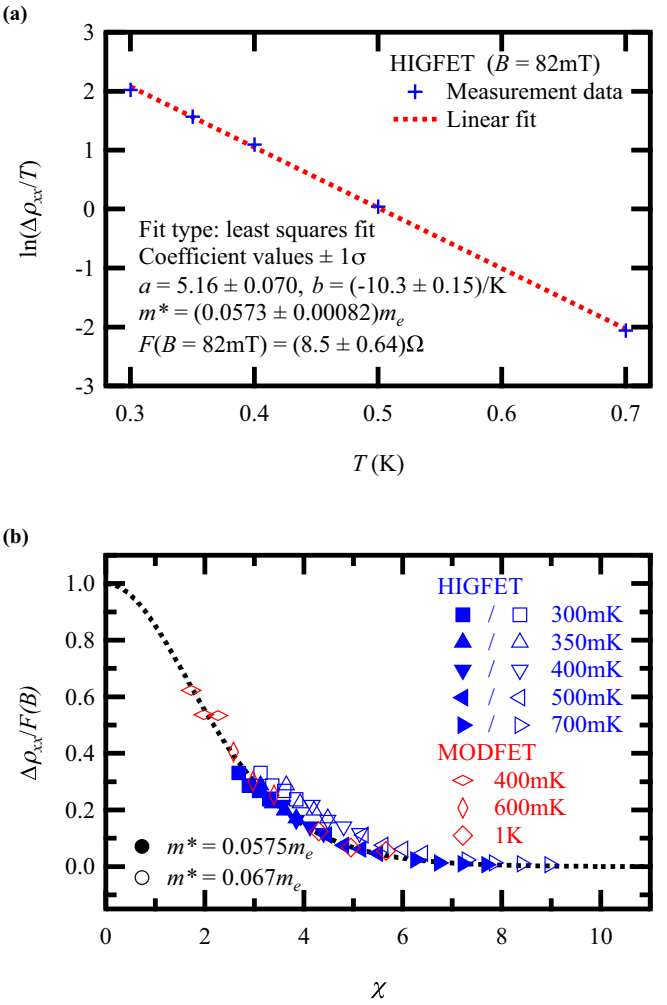

FIG. 4. $m^\star$ from a linear fit to the SdH oscillation amplitude at a density of $n = 6.1 \times 10^{10}\,\mathrm{cm}^{-2}$. (a) Linear fit to $\ln(\Delta\rho_{xx}/T)$ versus T for the SdH minimum at $B = 82$ mT of the HIGFET structure providing the effective mass $m^\star$ and the term $F(B = 82\,\mathrm{mT})$ (temperature range of 300 mK $\leqslant T \leqslant$ 700 mK). (b) With the determined reduced effective mass for the HIGFET structure (averaged over different minima in the field range of 75 mT $\leqslant B \leqslant$ 100 mT) of $m^\star = 0.0575\,m_e$ (solid symbols), the temperature dependence $\Delta\rho_{xx}/F(B)$ of the oscillation minima depicted as a function of χ collapses into $\chi/\sinh(\chi)$ (dotted line); by contrast, $\Delta\rho_{xx}/F(B) > \chi/\sinh(\chi)$ for all minima if an effective mass of $m^\star = 0.067\,m_e$ is assumed (open symbols). In the MODFET structure, no mass reduction occurs; accordingly, all open rhombi, representing the temperature dependence of the minima (170 mT $\leqslant B \leqslant$ 240 mT and 400 mK $\leqslant T \leqslant$ 1 K) with $\chi = \chi(m^\star = 0.067\,m_e)$, lie on the dotted line.

of the SdH minima is well described by $\chi/\sinh(\chi)$ and $\chi = \chi(m^\star = 0.067\,m_e)$.

While $m^\star$ is taken from the slope of the linear fit, the intercept gives the field dependent quantity $F(B)$ [cf. Fig. 4(a)]. The exponential factor in $F(B)$ [cf. Eqs. (8) and (9), respectively] is less robust concerning quantum localization, not considered in Eq. (6), than the temperature dependent part of the LK formula [43,59]. Therefore the determination of τ_q requires that the SdH oscillations be analyzed in the appropriate ranges

TABLE I. Fitting results for τ_q and the correction factor c according to a Lorentzian and a Gaussian shape of the DOS, respectively.

HIGFET	Lorentzian	Gaussian
τ_q	(7.3 ± 0.29) ps	(9.4 ± 0.28) ps
c	1.04 ± 0.067	0.46 ± 0.022
MODFET	Lorentzian	Gaussian
τ_q	(0.9 ± 0.12) ps	(2.3 ± 0.10) ps
c	50 ± 42	2.1 ± 0.62

of temperature and magnetic field. As compared to the first fitting procedure illustrated in Fig. 4(a), the temperature range was reduced to $300\,\text{mK} \leqslant T \leqslant 500\,\text{mK}$ since the very low oscillation amplitude at 700 mK would result in large relative errors of the fitting quantities. In addition, only SdH minima between 75 and 90 mT were taken into account since at the lower temperature boundary of 300 mK, deviations from Eq. (6) arise for magnetic fields $B \gtrsim 90\,\text{mT}$ (see Appendix B).

The nature of the Landau level broadening determines the shape of the density of states, which can either be Gaussian-like or a Lorentzian-like. Table I summarizes the results for τ_q and the correction factor c for both a Lorentzian (linear) and a Gaussian (parabolic) fit to the $\ln(F(B)/\rho_0)$ versus B^{-1} curve. The correction factor, c, is an indicator for the underlying shape of the DOS. For the HIGFET, the correction factors for both Lorentzian and Gaussian are close to one, thus making either one a compatible model.[2] The quantum scattering time, τ_q, is of the order of 10 ps in the HIGFET structure. In the case of the MODFET structure, the quadratic fit delivers a correction factor of $c \approx 2$, i.e., the DOS has a Gaussian shape and $\rho_{xx} \propto D(E_F)^2$. The linear fit connected to a Lorentzian shape does not provide reasonable results. This is in agreement with the calculations by Raikh and Shahbazyan [60], who have shown that in case of long-range scattering, e.g., from RI, and high Landau levels, their broadening is actually Gaussian.

Since even small perturbations lead to a dephasing of the cyclotron orbits [31] resulting in vanishing SdH oscillations, the onset of the oscillation (at the lowest accessible temperature) can be taken as a measure of τ_q, in the form of a lower boundary $\tau_q^{\text{onset}} = m^\star/2eB^{\text{onset}}$ if the SdH oscillations start at the magnetic field B^{onset} [22,61]. With $m^\star = 0.0575\,m_e$ and $B^{\text{onset}} = 30\,\text{mT}$, we obtained $\tau_q^{\text{onset}} = 5.5\,\text{ps}$ as a lower boundary, in agreement with the fitting results of $\tau_q \lesssim 10\,\text{ps}$ (Table I). In the MODFET structure, the SdH oscillation start at 118 mT resulting in $\tau_q^{\text{onset}} = 1.6\,\text{ps}$. This lower estimate is compatible with the result of of the Gaussian fit $\tau_q = 2.3\,\text{ps} \pm 0.10\,\text{ps}$ (cf. Table I).

[2]The correction factor $c = 1.04 \pm 0.067$, obtained from the intercept of the Lorentzian fit, is in agreement with the two assumptions of Eq. (6): (i) Lorentzian shape and a prefactor of ≈ 2, based on $\rho_{xx} \propto D(E_F)$, provided that the resistivity measured at $B = 0$ equals ρ_0. (ii) Lorentzian shape and a prefactor 4 (giving a correction factor $c = 1$), if the measured value is about twice ρ_0; alternatively, a Gaussian shape ($c \approx 0.5$) and a prefactor 2. A ρ_0 of half the measured value is unlikely because it would double the mobility determined to $\mu = 5.3 \times 10^6\,\text{cm/Vs}$ at $n = 6.1 \times 10^{10}\,\text{cm}^{-2}$.

Comparing the transport to the quantum scattering times for the HIGFET and the MODFET structure, provided that the resistivities measured at zero field equal the respective ρ_0, yields a ratio of $\tau_t/\tau_q \approx 18$ for both structures. In the case of the HIGFET, the upper estimate of $\tau_q = 10\,\text{ps}$ was used to calculate the ratio. Applying the smaller values of Table I, this ratio becomes even larger. Thus, based on the scattering-time ratio, there is the same dominant scattering mechanism—RI, according to Ref. [19]. However, the nature of the remote impurities is different in the HIGFET and the MODFET structure. Dopants, constituting the RI in the MODFET structure, are absent in the HIGFET structure, but there is an unavoidable surface charge in metal-gated undoped structures. It has been shown in theory [22] and experiment [62] that this surface charge may affect the 2DES similarly to the dopants in a modulation doped structures. Our results confirm that at the investigated density, the quantum scattering time in a HIGFET structure is dominated by the surface charge while the mobility is determined by BI scattering (cf. Fig. 2).

B. Fractional quantum Hall states

Fractional quantum Hall states emerge as a result of strong electron-electron interactions. The number and development of fractional quantum Hall states therefore critically depend on the quality of the sample, or, more precisely, on the impact of scattering on the electron interaction. Figure 5 therefore compares the HIGFET and the MODFET structure in terms of FQH states.

The MODFET sample has very low doping, resulting in an intrinsic density of only $n \approx 0.24 \times 10^{11}\,\text{cm}^{-2}$ and a small number of RI. Using the surface gate and the top gate, respectively, we adjusted the electron density in both the MODFET and HIGFET structure to $n \approx 0.6 \times 10^{11}\,\text{cm}^{-2}$ [red and black curve in Fig. 5(a)]. The HIGFET, not affected by RI, displays a significant number of well-developed FQH states at $T \approx 100\,\text{mK}$. Due to the low intrinsic electron density in the Hall-bar arms of the MODFET, not affected by the surface gate, only the low magnetic-field range is experimentally accessible. To allow direct comparison, we added data taken after low temperature LED illumination on another chip without surface gate from the same wafer, where the light can reach the 2DES unimpeded by the gold layer. The illumination facilitates the access to higher magnetic fields due to a decrease of localization in the contact arms. The field dependence of ρ_{xx} remains unchanged for $\nu \geqslant 1$ [blue and red curve in Fig. 5(a)], while for $\nu < 1$, various FQH states become visible. Compared to the dark HIGFET structure, the number of developed FQH states remains smaller in the full magnetic-field range, directly reflecting the impact of the RI scatterers. In addition, the widths of the integer quantum Hall states is significantly broader in the MODFET, another indicator of higher disorder in the doped structure. Since the scattering mechanisms in a HIGFET and MODFET are fundamentally different, and since the mobility depends on both the electron density and scattering, Fig. 5(a) can only compare magneto-transport for matching (low) densities. In Appendix C, an additional doped reference structure has been fabricated that matches the mobility of the HIGFET at $n \approx 1.3 \times 10^{11}\,\text{cm}^{-2}$. Transport measurements demonstrate

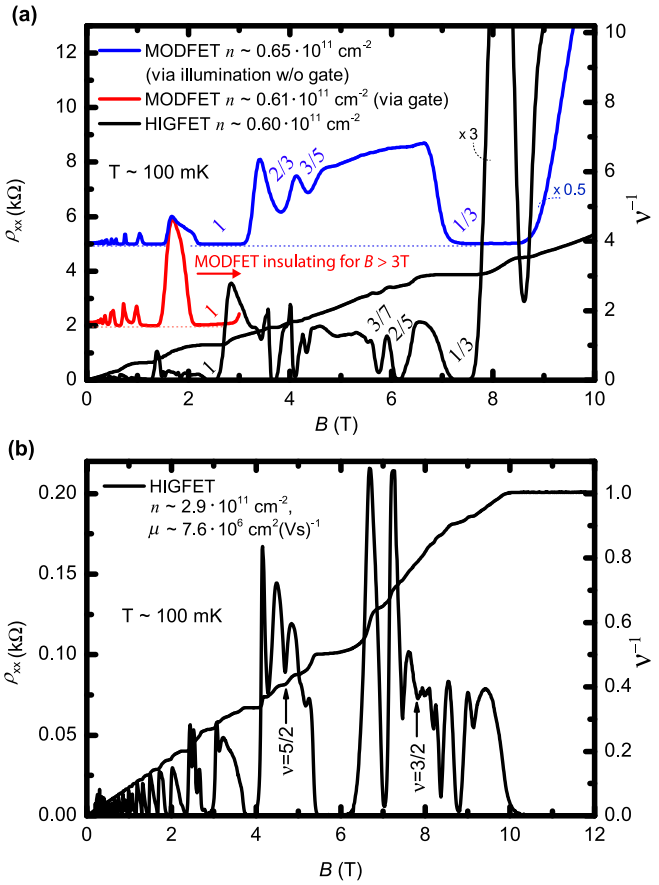

FIG. 5. Comparison of the longitudinal resistivity ρ_{xx} and the Hall resistivity (expressed as the inverse filling factor $\nu^{-1} \propto \rho_{xy}$) of the HIGFET and the MODFET structure at $T \approx 100$ mK. (a) At low electron density of $n \approx 0.6 \times 10^{11}$ cm^{-2}, the HIGFET structure shows various well-developed FQH states (black solid line). Due to the low intrinsic density of the ungated contact arms in the MODFET, only the low magnetic-field range is accessible (red solid line). After LED illumination (different chip of the same wafer without surface gate), a few fractional states start to develop in the MODFET structure. The corresponding electron mobilities are $\mu \approx 1.4 \times 10^6$ cm^2/Vs (MODFET illuminated), $\mu \approx 0.9 \times 10^6$ cm^2/Vs (MODFET gated), and $\mu \approx 5.4 \times 10^6$ cm^2/Vs (HIGFET). The curves were scaled up or down to simplify comparison. (b) Highest accessible density in the HIGFET structure before gate hysteresis arises. In this density regime, the 5/2 state develops and several FQH states in the vicinity of $\nu = 3/2$ are visible.

also under these conditions that the HIGFET structure is superior to its doped counterpart.

Figure 5(b) shows the HIGFET at the highest density of $n \approx 2.9 \times 10^{11}$ cm^{-2} before gate hysteresis arises. A large number of FQH states in the vicinity of $\nu = 3/2$ and the onset of a 5/2 state are visible.

V. CONCLUSION

In summary, we have investigated the impact of remote ionized impurity scattering on the quality of a two-dimensional electron gas. Various measures have been examined in the absence of remote impurities in a HIGFET structure and compared to a MODFET structure grown under identical conditions. Our results indicate that, regardless of the chosen criterion, the elimination of RI is clearly accompanied by a quality enhancement of the 2DES hosted in a single-interface GaAs/AlGaAs heterostructure. This quality enhancement is particularly noticeable in the low-density regime with electron densities accessible down to 8×10^9 cm^{-2} after illumination.

Based on the mobility-density dependence, ionized background impurities (at low densities) and interface roughness (at high densities) have been found to be the dominant sources of scattering in our HIGFET structure, in agreement with Ref. [14]. The MODFET structure, however, is dominated by remote ionized impurities over the full density range. At comparable densities, several FQH states including the 5/2 state only form in the HIGFET structure. At an investigated electron density of about 6×10^{10} cm^{-2}, the effective electron mass is reduced by 14% with respect to the bulk band mass in GaAs, producing strong evidence for electron-electron interaction. The obtained values of the quantum scattering times, based on the SdH oscillation amplitude, are higher by a factor of approximately four than in the MODFET structure. The comparison of the zero-field transport scattering times at that density yields a similar ratio, which is equivalent to a comparable ratio of transport and quantum scattering time for both structures. Hence, our measurements show the dichotomy between mobility and quantum scattering time in HIGFET structures—μ is predominantly affected by BI, τ_q by surface charge (at the considered electron density).

ACKNOWLEDGMENTS

We would like to acknowledge Francois Sfigakis for discussion and especially for sharing the knowledge about the processing of HIGFET structures accumulated at Cavendish Laboratory. Helpful discussions with Thomas Feil and Werner Dietsche were highly appreciated. This work was supported by the Swiss National Science Foundation (SNF).

APPENDIX A: α PARAMETER

1. Double-logarithmic plot of the mobility-density dependence

As a supplement to Fig. 2, Fig. 6 shows the $\log_{10}(\mu)$ versus $\log_{10}(n)$ plot, whose linear slope provides the α parameter giving insight into the nature of the dominant scattering mechanism.

2. Fourier analysis at high density

A Fourier analysis of the SdH oscillations at an electron density of 2.9×10^{11} cm^{-2}, i.e., beyond the peak mobility of the HIGFET structure. The existence of a single peak confirms that only the lowest subband is occupied (cf. Fig. 7) and that the decreasing mobility [cf. Fig. 2(a)] cannot be attributed to intersubband scattering.

APPENDIX B: DEVIATION FIELD

Ando's zero temperature theory [34] is limited by a critical $\omega_c \tau_q \approx 0.8$, above which higher-order corrections become necessary. This can be translated into an upper validity

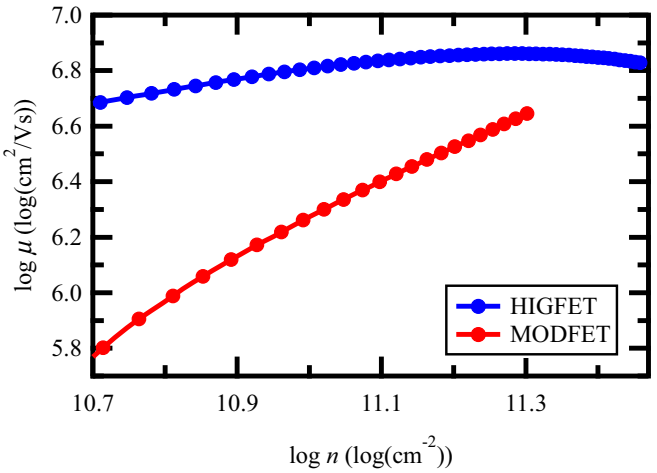

FIG. 6. Double-$\log_{10}$ plot of the mobility-density dependence of the 2DES in the MODFET (red) and HIGFET (blue) structure shown in Fig. 2(a). The values $\alpha(n)$ [cf. Fig. 2(b)] are obtained from the linear slope of this $\log_{10}(\mu)$ vs $\log_{10}(n)$ plot.

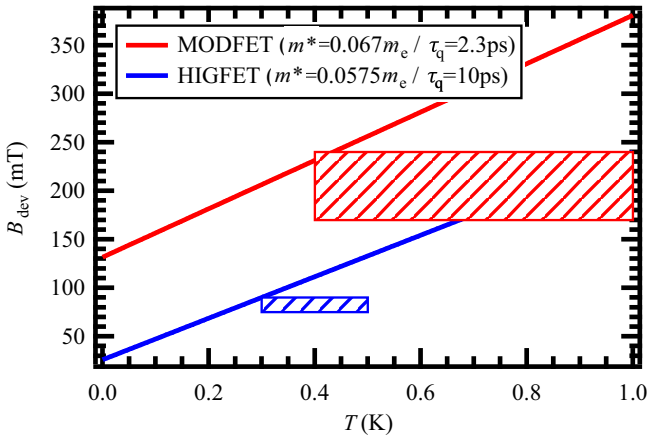

FIG. 8. Deviation field as a function of temperature, calculated with the values of $m^\star$ and τ_q of the HIGFET (blue) and the MODFET (red) structure. Above the respective lines deviations from Eq. (6) are expected. The rectangles represent the field and temperature ranges where the SdH oscillations were analyzed in order to obtain $m^\star$ and τ_q, underlining the applicability of the LK formula in those ranges.

limitation

$$\frac{1}{2\pi\omega_c\tau_q} \gtrsim 0.2\,. \tag{B1}$$

At finite temperature, this limitation can be generalized [50] to

$$\frac{1}{2\pi\omega_c\tau_q} + \frac{k_B T}{\hbar\omega_c} \gtrsim 0.2\,. \tag{B2}$$

Accordingly, there is a critical magnetic field

$$B_{\rm dev} \approx 5\frac{m^\star}{e}\left(\frac{1}{2\pi\tau_q} + \frac{k_B}{\hbar}T\right), \tag{B3}$$

above which deviations to Eq. (6) occur, and which is proportional to $m^\star$, decreasing with increasing τ_q, and rising with temperature.

Figure 8 shows the temperature dependence of the deviation field, based on the values of $m^\star$ and τ_q obtained from the two consecutive fits described above. Due to the reduced effective mass and the higher quantum scattering time, this deviation field $B_{\rm dev}$ is lower for the HIGFET structure and in the order of the examined field range. Higher temperatures would increase the deviation field but also raise the field range where SdH oscillations occur and can be analyzed according to the LK formula.

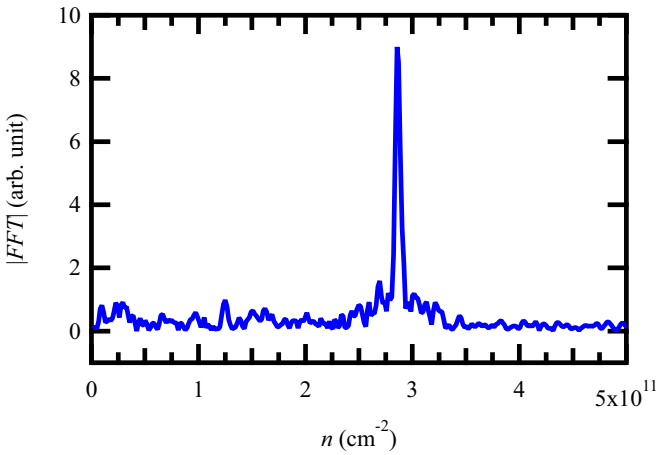

FIG. 7. Fourier analysis of the SdH oscillations in the HIGFET structure at a density of 2.9×10^{11} cm^{-2}, revealing the occupation of only the lowest 2D subband.

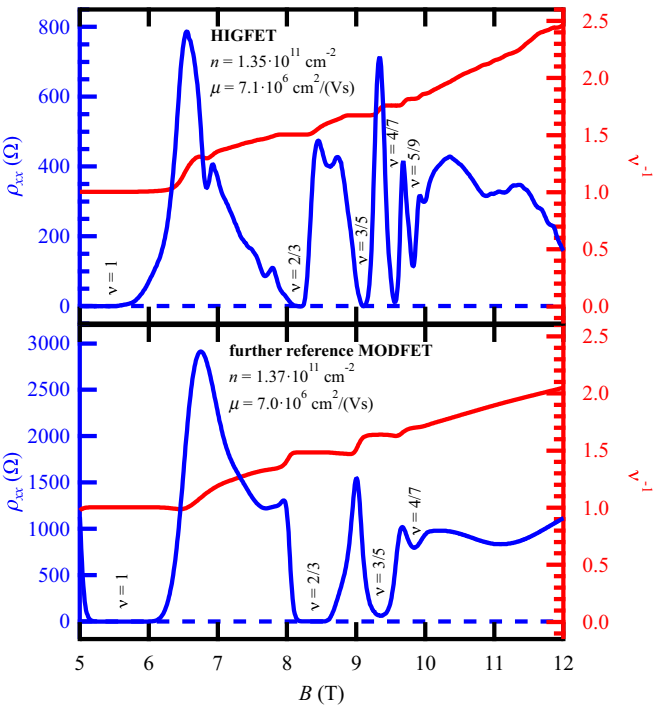

FIG. 9. Magnetotransport showing FQH states in the lowest Landau level in the HIGFET structure (top) and a doped reference structure in van der Pauw geometry (bottom) of comparable mobility ($T \lesssim 100$ mK). The sample was not illuminated.

APPENDIX C: FQH STATES AT COMPARABLE MOBILITIES

Figure 9 compares magnetotransport between the existing HIGFET structure to another doped structure of comparable mobility (at intermediate density). Also for matching mobilities, the HIGFET exhibits more and better developed FQH states. The state at filling factor $\nu = 4/7$ is fully developed and in contrast to the MODFET, the $\nu = 5/9$ state is visible. We can clearly attribute the more pronounced FQH states in undoped heterostructures to the absence of remote ionized impurities.

[1] D. C. Tsui, H. L. Stormer, and A. C. Gossard, Phys. Rev. Lett. **48**, 1559 (1982).
[2] R. B. Laughlin, Phys. Rev. Lett. **50**, 1395 (1983).
[3] H. Stormer, Rev. Mod. Phys. **71**, 875 (1999).
[4] R. Willett, J. P. Eisenstein, H. L. Störmer, D. C. Tsui, A. C. Gossard, and J. H. English, Phys. Rev. Lett. **59**, 1776 (1987).
[5] V. Umansky, M. Heiblum, Y. Levinson, J. Smet, J. Nübler, and M. Dolev, J. Cryst. Growth **311**, 1658 (2009).
[6] C. Reichl, J. Chen, S. Baer, C. Rössler, T. Ihn, K. Ensslin, W. Dietsche, and W. Wegscheider, New J. Phys. **16**, 023014 (2014).
[7] K.-J. Friedland, R. Hey, H. Kostial, R. Klann, and K. Ploog, Phys. Rev. Lett. **77**, 4616 (1996).
[8] C. Reichl, Ph.D. thesis, ETH, Zürich, 2014.
[9] G. Gamez and K. Muraki, Phys. Rev. B **88**, 075308 (2013).
[10] M. Samani, A. V. Rossokhaty, E. Sajadi, S. Lüscher, J. A. Folk, J. D. Watson, G. C. Gardner, and M. J. Manfra, Phys. Rev. B **90**, 121405 (2014).
[11] R. H. Harrell, K. S. Pyshkin, M. Y. Simmons, D. A. Ritchie, C. J. B. Ford, G. A. C. Jones, and M. Pepper, Appl. Phys. Lett. **74**, 2328 (1999).
[12] B. E. Kane, L. N. Pfeiffer, K. W. West, and C. K. Harnett, Appl. Phys. Lett. **63**, 2132 (1993).
[13] B. E. Kane, L. N. Pfeiffer, and K. W. West, Appl. Phys. Lett. **67**, 1262 (1995).
[14] S. Sarkozy, K. Das Gupta, C. Siegert, A. Ghosh, M. Pepper, I. Farrer, H. E. Beere, D. A. Ritchie, and G. A. C. Jones, Appl. Phys. Lett. **94**, 172105 (2009).
[15] F. Sfigakis, K. Das Gupta, S. Sarkozy, I. Farrer, D. A. Ritchie, M. Pepper, and G. A. C. Jones, Physica E **42**, 1200 (2010).
[16] W. Pan, H. L. Stormer, D. C. Tsui, L. N. Pfeiffer, K. W. Baldwin, and K. W. West, Solid State Commun. **119**, 641 (2001).
[17] W. Pan, N. Masuhara, N. S. Sullivan, K. W. Baldwin, K. W. West, L. N. Pfeiffer, and D. C. Tsui, Phys. Rev. Lett. **106**, 206806 (2011).
[18] W. Y. Mak, K. Das Gupta, H. E. Beere, I. Farrer, F. Sfigakis, and D. A. Ritchie, Appl. Phys. Lett. **97**, 242107 (2010).
[19] S. J. MacLeod, K. Chan, T. P. Martin, A. R. Hamilton, A. See, A. P. Micolich, M. Aagesen, and P. E. Lindelof, Phys. Rev. B **80**, 035310 (2009).
[20] E. H. Hwang and S. Das Sarma, Phys. Rev. B **77**, 235437 (2008).
[21] V. Umansky, R. de Picciotto, and M. Heiblum, Appl. Phys. Lett. **71**, 683 (1997).
[22] S. Das Sarma and E. H. Hwang, Phys. Rev. B **90**, 035425 (2014).
[23] P. Drude, Ann. Phys. **306**, 566 (1900).
[24] J. H. Davies, *The Physics of Low-Dimensional Semiconductors* (Cambridge University Press, Cambridge, 1997).
[25] S. Das Sarma and F. Stern, Phys. Rev. B **32**, 8442 (1985).
[26] A. Gold, Phys. Rev. B **38**, 10798 (1988).
[27] K. Lee, M. S. Shur, T. J. Drummond, and H. Morkoc, J. Appl. Phys. **54**, 6432 (1983).
[28] D. Reuter, M. Versen, M. D. Schneider, and A. D. Wieck, J. Appl. Phys. **88**, 321 (2000).
[29] T. Saku, Y. Horikoshi, and Y. Tokura, Jpn. J. Appl. Phys. **35**, 34 (1996).
[30] S. Das Sarma and B. Vinter, Phys. Rev. B **24**, 549 (1981); Surf. Sci. **113**, 176 (1982).
[31] J. P. Harrang, R. J. Higgins, R. K. Goodall, P. R. Jay, M. Laviron, and P. Delescluse, Phys. Rev. B **32**, 8126 (1985).
[32] B. A. Piot, D. K. Maude, M. Henini, Z. R. Wasilewski, K. J. Friedland, R. Hey, K. H. Ploog, A. I. Toropov, R. Airey, and G. Hill, Phys. Rev. B **72**, 245325 (2005).
[33] T. Ando and Y. Uemura, J. Phys. Soc. Jpn. **36**, 959 (1974).
[34] T. Ando, J. Phys. Soc. Jpn. **37**, 1233 (1974).
[35] I. M. Lifshitz and A. M. Kosevich, Sov. Phys. JETP **2**, 636 (1956).
[36] R. B. Dingle, Proc. R. Soc. London A **211**, 517 (1952).
[37] T. Ando, J. Phys. Soc. Jpn. **51**, 3900 (1982).
[38] A. Isihara and L. Smrcka, J. Phys. C **19**, 6777 (1986).
[39] P. T. Coleridge, R. Stoner, and R. Fletcher, Phys. Rev. B **39**, 1120 (1989).
[40] P. T. Coleridge, P. Zawadzki, and A. S. Sachrajda, Phys. Rev. B **49**, 10798 (1994).
[41] P. T. Coleridge, Semicond. Sci. Technol. **12**, 22 (1997).
[42] P. T. Coleridge, Semicond. Sci. Technol. **5**, 961 (1990).
[43] D. R. Hang, C. F. Huang, and K. A. Cheng, Phys. Rev. B **80**, 085312 (2009).
[44] S. Sarkozy, K. Das Gupta, F. Sfigakis, H. Beere, I. Farrer, R. Harrell, D. A. Ritchie, and G. A. C. Jones, ECS Trans. **11**, 75 (2007).
[45] M. Shayegan, V. J. Goldman, C. Jiang, T. Sajoto, and M. Santos, Appl. Phys. Lett. **52**, 1086 (1988).
[46] M. Shayegan, V. J. Goldman, M. Santos, T. Sajoto, L. Engel, and D. C. Tsui, Appl. Phys. Lett. **53**, 2080 (1988).
[47] M. A. Paalanen, D. C. Tsui, and J. C. M. Hwang, Phys. Rev. Lett. **51**, 2226 (1983).
[48] S. Chakravarty and A. Schmid, Phys. Rep. **140**, 193 (1986).
[49] K. K. Choi, D. C. Tsui, and S. C. Palmateer, Phys. Rev. B **33**, 8216 (1986).
[50] M. Hayne, A. Usher, J. J. Harris, and C. T. Foxon, Phys. Rev. B **46**, 9515 (1992).
[51] Y.-W. Tan, J. Zhu, H. L. Stormer, L. N. Pfeiffer, K. W. Baldwin, and K. W. West, Phys. Rev. Lett. **94**, 016405 (2005).
[52] A. T. Hatke, M. A. Zudov, J. D. Watson, M. J. Manfra, L. N. Pfeiffer, and K. W. West, Phys. Rev. B **87**, 161307 (2013).
[53] Y. Zhang and S. Das Sarma, Phys. Rev. B **72**, 075308 (2005).
[54] A. P. Smith, A. H. MacDonald, and G. Gumbs, Phys. Rev. B **45**, 8829 (1992).
[55] R. Asgari and B. Tanatar, Phys. Rev. B **74**, 075301 (2006).
[56] Y. Kwon, D. M. Ceperley, and R. M. Martin, Phys. Rev. B **50**, 1684 (1994).

[57] N. D. Drummond and R. J. Needs, Phys. Rev. B **87**, 045131 (2013).
[58] A. Usher, R. J. Nicholas, J. J. Harris, and C. T. Foxon, Phys. Rev. B **41**, 1129 (1990).
[59] D. Hang, C. Huang, Y. Zhang, H. Yeh, J. Hsiao, and H. Pang, Solid State Commun. **141**, 17 (2007).
[60] M. E. Raikh and T. V. Shahbazyan, Phys. Rev. B **47**, 1522 (1993).
[61] J. Falson, Y. Kozuka, J. H. Smet, T. Arima, A. Tsukazaki, and M. Kawasaki, Appl. Phys. Lett. **107**, 082102 (2015).
[62] D. Q. Wang, J. C. H. Chen, O. Klochan, K. Das Gupta, D. Reuter, A. D. Wieck, D. A. Ritchie, and A. R. Hamilton, Phys. Rev. B **87**, 195313 (2013).